GAS DYNAMICS OF LASER PLASMA IN THE COURSE OF HEATING

N. G. BASOV, V. A. BOĬKO, V. A. GRIBKOV, S. M. ZAKHAROV, O. N. KROKHIN, and G. V. SKLIZKOV

P. N. Lebedev Physics Institute, USSR Academy of Sciences

Submitted February 26, 1971

Zh. Eksp. Teor. Fiz. 61, 154–161 (July, 1971)

Gas dynamic properties of laser plasma formed by an intense laser beam focused on the surface of a carbon target are investigated experimentally. The time dependence of plasma pressure in the heating region, of the mass flow from the target surface, and of the mass of heated plasma are measured by the method of slit scanning of the interference pattern by an image converter. The gas dynamic processes in hot plasma are discussed. In the case of a multimode Q-switched laser the maximum plasma pressure is found to occur at the beginning of the pulse. The maximum plasma pressure reaches 10^6 atm.

AT this time there are two approaches to the problem of heating plasma to thermonuclear temperatures by laser radiation[1]: (1) the inertial containment method, in which a sufficient amount of energy is coupled to the plasma to heat it to thermonuclear temperatures in time not exceeding the gas dynamic acceleration time, and (2) the gas-dynamic motion method (in which the laser pulse length significantly exceeds the inertial time) where a significant potion of laser energy is transformed into the energy of directed gas-dynamic motion. The second method can be used for collision and cumulation of laser-derived plasma flows to increase the ionic temperature and lifetime of plasma[2]. The initial stage of plasma motion is particularly significant in the heating process because, first, it determines the electric density gradient near the surface of the condensed material that governs the efficiency of the heat energy coupling, and second, it is at the initial stage that a significant gas-dynamic acceleration of plasma takes place.

A number of authors (see[3–5] for example) have determined the parameters of laser plasma mainly as quantities averaged over the time of action of the radiation pulse. In[6,7] the time dependence of volume-averaged electronic temperature of plasma was determined from x-ray radiation. We note the contradictory nature of the data reported in these studies. Beside the electronic temperature, the significant parameters describing the plasma heating process are the mass flow and the pressure, and their dependence on radiation power. At this time there are no reports on the measurements of plasma pressure on a solid target. In[8] this pressure was estimated from a recoil momentum and represented a value averaged over the time of ejection of the heated material. In this case, as shown in[9], for large mass flows the major portion of the pulse is spent on the "cold" material ejected after the expansion of hot plasma. The total momentum carried away by the plasma was determined merely from interferometric measurements of the mass and velocity of plasma after the passage of the laser pulse. However, to understand the plasma heating process it is necessary to know not only the values of the total mass and momentum of the heated plasma but also, in the first place, their time variation during the action of the laser pulse and their dependence on the intensity
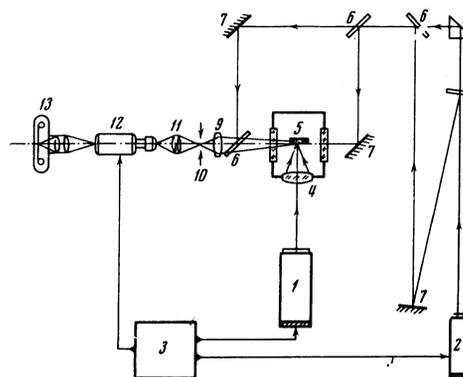
FIG. 1. Diagram of a setup for time scan of flare interferogram using an image converter. 1—neodymium laser; 2—ruby laser; 3—control unit; 4—focusing lens; 5—target; 6—beam splitters; 7—mirrors; 8—prism; 9—lens for projecting interference image on the slit; 10 and 11—lens for projecting slit image on photocathode; 12—photoelectric recorder; 13—camera.

of the heating radiation. Therefore this paper reports the first attempt to measure the density and velocity distributions of a plasma and to evaluate the mass flow from the surface and plasma pressure in the target heating process, based on high-speed interferometric measurements.

1. METHOD OF MEASUREMENTS AND EXPERIMENTAL SETUP

The experimental setup (Fig. 1) consisted of a neodymium glass laser for heating plasma and a ruby laser serving as a pulse source for the interferometer.

FIG. 2. Time scan of the interference pattern of a carbon flare. The slit of an electron-optical recorder coincides with the neodymium laser beam axis and is perpendicular to target surface. The interference bands in zero location are oriented parallel to the target. r—distance from the target; r = 0 corresponds to target surface. Below is an oscilloscopic trace of the heating pulse. The region bounded by the r = 0 axis and the interference bands corresponds to the opacity zone.

81
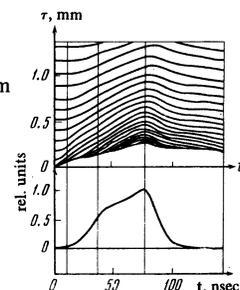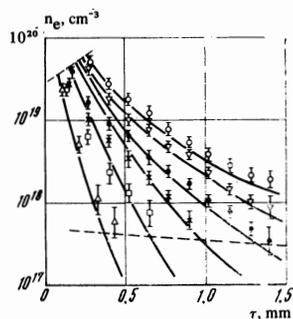
FIG. 3. Electron density distribution along the axis of a laser beam at various times reckoned from the beginning of the laser pulse (in nanoseconds): $\triangle - t = 10$; $\square - t = 16$; $\times - t = 23$; $\bullet - t = 36$; $\nabla - t = 56$; $\bigcirc - t = 76$.

The ruby laser pulse used for illumination was lengthened by a multipath optical delay line.

The massive carbon target was placed in vacuum at a pressure not exceeding 10^{-5} mm Hg. The energy of the neodymium laser was 8 J for a total length of 80 nsec at the 0.1 amplitude level. The pulse oscillogram is shown in Fig. 2. The maximum divergence of the beam corresponding to maximum intensity was 2×10^{-3} rad. The divergence at the pulse front increased approximately linearly with intensity while the radius of the focal spot varied from 0.05 to 0.2 mm (the caustic radius of the focusing lens was 0.05 mm).

The interferometer was tuned according to the Mach-Zender system. The slit image of the interferogram was time scanned by means of an FÉR-1 scanning camera with a spatial resolution of 20 lines/mm at the cathode and a time resolution of ~ 0.2 nsec[10]. Using a total magnification of $14 \times$ and a spatial resolution of 7 lines/mm at the electron-optical converter screen, the interference patterns were measured accurate to $\frac{1}{3}$ band in the region of maximum band density and at least to $\frac{1}{20}$ band at the edge of the expanding plasma. In time scans of the interference patterns the bands were oriented parallel to the target while the slit was perpendicular to target surface and coincided with the beam axis. For measurements the interferogram cross section was broken down into 10 zones with a 0.1 mm pitch. The interferograms were processed by the parabolic method, assuming axial symmetry[11].

Figure 2 shows a typical time scan of the interference pattern. It is apparent that the zone opaque to the illuminating beam expands in time and reaches a maxi-

mum magnitude of ~ 0.25 mm 76 nsec after the effective onset of the heating pulse. At that time the value of electron density at the boundary of this zone is $\sim 5 \times 10^{19}$ cm^{-3}. The interferogram was used to determine the electron-density profiles for various instants of time (Fig. 3). The points at the beginning and the end of each line designate the limiting values of density that can be measured quantitatively by this method.
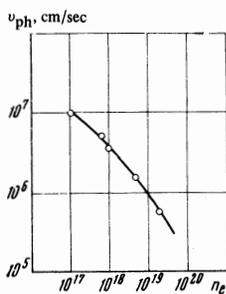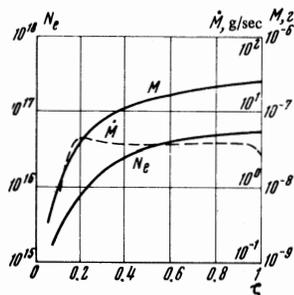
2. MOTION OF MATTER AND MASS FLOW FROM THE SURFACE

The graphs in Fig. 3 were used to plot r—t diagrams of motion of points of a plasma having a given density. These diagrams turned out to be straight lines within the heating pulse front and were used to determine the velocity of motion of the aforementioned points (Fig. 4). For example, the boundary velocity of plasma with $n_e = 10^{17}$ cm^{-3} was 10^7 cm/sec. In this connection we emphasize two considerations. First, according to the results of interference pattern analysis (Figs. 3 and 4) the boundary velocity of plasma of a given density is approximately constant over the entire leading front of the laser pulse. Second, none of these velocities is exactly the mass velocity of the matter, and merely approximately reflects the motion of the matter within the flare. As a rule such a "phase" velocity is lower than mass velocity at the given point. The mass velocity can be measured more exactly by the method of the Doppler shift of the self-inverted line[12].

The total mass of plasma heated at a given time was determined by integrating the lines in Fig. 3. The missing sectors of the lines were approximated by the expression

$$n_e = \frac{10^{17}}{R^2} \frac{(1-\xi)^\alpha}{\xi^2}, \tag{1}$$

where $\xi = (r + 0.01)R^{-1}$; r is the distance from the focusing point, $R = v_{max}t$ is the radius of plasma boundary, and v_{max} is the asymptotic velocity of the plasma particles. The plasma expansion is assumed to be spherically symmetric. The best simultaneous approximation for all lines is reached for the exponent $\alpha \approx 16$. We see that the plasma velocity gradient in the heated region is large and decreasing with time as $\sim t^{-3}$. The time dependence of plasma mass is shown in Fig. 5. The same figure shows a plot of the "vaporization" rate $\dot{M}$, whose maximum turns out to equal ~ 4 g/sec.

3. THE OPACITY ZONE

A typical feature of all high-speed photographs of the flare in laser light is the opacity zone next to the target. The nature of this zone is still not fully understood. The electron density at the boundary of this zone is $\sim 5 \times 10^{19}$ cm^{-3}, a value significantly lower than the critical point. Consequently the reflection of the illuminating beam from plasma with critical density cannot be the cause of darkening of this portion of the interferogram.

We now consider the refraction of illuminating beams within the opacity zone. According to Fig. 3 the boundary of this zone shows large density gradients causing a strong refraction. It is estimated that for a

FIG. 4

FIG. 5

FIG. 4. Phase velocity v_{ph} of fixed-density regions.

FIG. 5. Plasma mass M, total number of electrons N_e, and mass flow $\dot{M}$ as functions of $\zeta = t/\tau$, where τ is the length of the leading front of the laser pulse.

beam path length of ~0.1 mm in the flare ~0.1 mm from target the angle of refraction determined by the expression

$$\varepsilon \approx \text{arctg} \int \frac{\partial}{\partial x} \ln n(xyz)\,dz,$$

exceeds $2°$; such rays fail to reach the image converter screen in our experimental geometry. Here the z axis coincides with the direction of the illuminating beam, the x axis is perpendicular to the target, and integration is carried over the entire path of the illuminating beam in plasma. Thus the refraction of the illuminating beam due to the sharp density gradient is one of the causes of the opacity zone appearing in interference patterns at $\lambda \approx 0.69\ \mu$ and at plasma densities significantly below critical.

On the other hand, the opacity zone can be due to the condensation of interference bands; up to ~100 bands are bent in this zone. For the dimensions of ~0.1 mm this means that bands in this zone merge into a continuous gray background. This phenomenon should appear mainly at a late heating stage corresponding to the trailing edge of the radiation pulse, when the density gradients near the target are decreased because of plasma expansion.

Nevertheless these considerations are inadequate as direct evidence of a smooth profile of electron density within the opacity zone, and additional experiments are needed for an exact determination of the state of matter in this zone.

4. DISCUSSION OF RESULTS

We consider the state of matter in the part of the flare inside the opacity zone, where strong absorption gives rise to plasma heating processes that determine the condition of the expanding plasma. Of definite interest is the determination of the pressure of plasma heated within the opacity zone; knowledge of the experimental values of the heated plasma pressure on the target and the mass flow permits us in principle to determine all gas dynamic parameters in any part of the flare from the boundary problem, eliminating solid-state parameters from consideration.

Data on the density and velocity profiles of individual plasma regions can be used to compute the momentum of moving plasma. Since the plasma is accelerated directly at the target the momentum uniquely determines plasma pressure on the target. We assume that the plasma expands with spherical symmetry and that during the action of the laser pulse the plasma boundary moves far beyond the diameter of the focusing spot. For the projection of the plasma momentum on a surface normal to the target surface we have

$$F(t) = \int \rho(r,t) v_n(r,t)\,dV, \qquad (2)$$

where $\rho(r,t) = n_e m_i / z$, m_i is ion mass, z is effective charge, $v_n(r,t)$ is velocity projection on the normal, and r is the distance from the center of the focusing spot. Integration extends over the entire volume.

Hence the pressure on target surface within the limits of the hot portion of the flare is

$$p(\zeta) = (\pi r_0^2 \tau)^{-1} dF / d\zeta, \qquad (3)$$

FIG. 6. Velocity profile of material in plasma along the axis of the laser beam. Here v_0 is the velocity of sound in plasma at the target, $r_1 = 0.06$ cm.
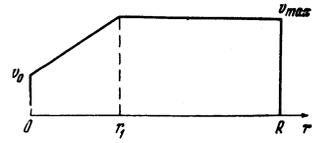
where r_0 is the radius of the focal spot, τ is the heating time, and $\zeta = t/\tau$ is dimensionless time.

The velocity profile $v(r)$ used in this computation is given in Fig. 6. This profile was chosen on the basis of experimental data obtained by Doppler shift measurements of plasma velocity[12] and of the results of time scans of the flight of differently charged ions in the light of the corresponding lines[13]. Considering that $v_0 \sim q^{1/4}$ (q is the radiation flux density), $r_0 = r_{0T}(\kappa_1 + \kappa_2\zeta)$, r_0 is the maximum value of the focal spot at time τ, κ_1 and κ_2 are 0.25 and 0.75 respectively. The expression for velocity is written here in the form

$$v = v_0(1 + \beta\xi)\ \text{for}\ r \leqslant r_1,$$
$$v = v_0(1 + \beta)\ \text{for}\ r_1 \leqslant r \leqslant R;$$
$$\beta = (v_{max} - v_0)/v_0\xi_1, \qquad (4)$$
$$v_0 = A_1\zeta^{1/4}(\kappa_1 + \kappa_2\zeta)^{-1/2},$$
$$v_{max} = \beta_1 v_0, \quad \beta_1 = 5, \quad \xi_1 = r_1/R.$$

For the case of neodymium laser with an emission pulse shown in Fig. 2 and pulse peak energy of 8 J ($\tau = 76$ nsec) we have the temperature $T \approx 50$ eV and the effective ionic charge $z \approx 5$. Here $A_1 = 0.5 \times 10^7$ cm/sec, $v_{max} = 2.5 \times 10^7$ cm/sec, and $r_0 = 2 \times 10^{-2}$ cm. The divergence of the laser beam increases linearly in time over a large portion of the pulse front. The angular and spatial characteristics of the light beam were investigated by the image converter slit scan method. To compute the pressure, the leading edge of the pulse was approximated by a linear function. Based on these assumptions, the pressure is computed from (3), in which the force impulse is determined from

$$F(\zeta) = 4.9\Phi_1(\xi_1)\Psi(\zeta),$$
$$\Phi_1(\xi_1) = 1 + 4.5\xi_1 - (1 - \xi_1)^{18}, \qquad (5)$$
$$\Psi(\zeta) = \zeta^{11/4}(\kappa_1 + \kappa_2\zeta)^{-3/2}.$$

Here the force acting on the target is determined by the impulse derivative
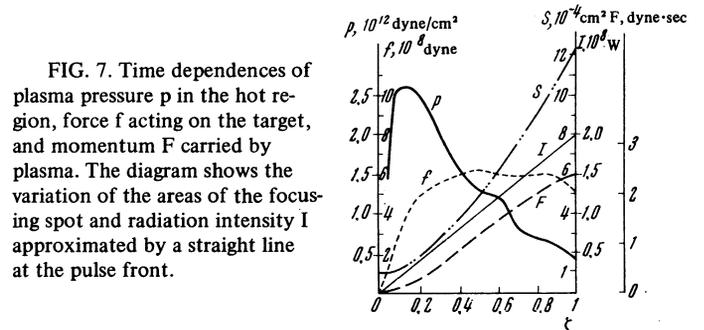
FIG. 7. Time dependences of plasma pressure p in the hot region, force f acting on the target, and momentum F carried by plasma. The diagram shows the variation of the areas of the focusing spot and radiation intensity I approximated by a straight line at the pulse front.

$$f(\zeta) = \frac{1}{\tau}\frac{dF(\zeta)}{d\zeta}. \qquad (6)$$

Figure 7 shows the curves of force impulse, force, and pressure of plasma on the target. We see that the maximum of pressure occurs at the beginning of the pulse because the divergence is small at low intensity and the focal spot diameter is determined merely by the lens caustic in this experiment. At later stages, according to Fig. 3, the density profile becomes elevated and the plasma region of absorption moves away from the target and increases. The gas mass directly heated by laser radiation also increases. The pressure drop indicates the occurrence of a peculiar screening of the laser radiation. The temperature in the hot region falls and an ever greater portion of radiation energy is transformed directly into kinetic energy of the expanding material.

Thus by varying the time dependence of the radiation divergence we can shift the pressure maximum and achieve optimal utilization of laser energy for heating plasma under real conditions. The presence of a pressure peak and consequently of a temperature peak at the beginning of the laser pulse explains the experimental results reported in[6] whose authors observed an intense peak of x-ray radiation from the flare at the very beginning of the laser pulse where the radiation power was much lower than maximal.

It should be noted that the inaccuracy in the determination of pressure is mainly due to the indeterminacy of the effective area subject to this pressure. In this experiment due to the spherical expansion and adiabatic motion of plasma beyond the focal spot this area cannot exceed the quantity $\pi r_0^2 \tau$ by a factor greater than 2–3. This inaccuracy in the determination of area does not affect the shape of the $p(t)$ function and affects only the absolute value of pressure.

As for the thermal pressure within the hot region, it is determined by the relation

$$p_\tau(t) = p(t) - \rho(0,t)v_0^2,$$

where $\rho(0,t)$ is the material density at the target surface. Assuming that $n_e \lesssim 5 \times 10^{20}$ cm^{-3} ($\rho(0,T) \approx 2 \times 10^{-3}$ g) we have for the kinetic part of pressure $\rho(0,t)v_0^2 \approx 5 \times 10^{10}$ dyne/cm^2. Thus the contribution of kinetic pressure in the hot region is small in comparison to thermal pressure.

[1] N. G. Basov and O. N. Krokhin, The Use of Lasers for Thermonuclear Fusion, Vestnik Akad. Nauk SSSR 6, 55 (1970).

[2] N. G. Basov, O. N. Krokhin, and G. V. Sklizkov. Formation of Shock Waves by High-power Laser Radiation. ZhETF Pis. Red. 6, 683 (1967) [JETP Lett. 6, 168 (1967)].

[3] N. G. Basov, O. N. Krokhin, and G. V. Sklizkov, Trudy FIAN 52, "Kvantovaya radio-fizika" ("Quantum Radiophysics"), p. 171, 1970.

[4] A. Haught and D. Polk, Phys. of Fluids 13, 2825 (1970).

[5] D. D. Burgess, B. C. Faucett, and N. G. Peacock, Proceedings of the Physical Society 92, 525 (1967).

[6] G. L. Bobin, F. Floux, P. Langer, and M. Pignerol, Phys. Lett. 28A, 398 (1968).

[7] N. G. Basov, V. A. Boĭko, V. A. Gribkov, S. M. Zakharov, O. N. Krokhin, and G. V. Sklizkov, ZhETF Pis. Red. 9, 520 (1969) [JETP Lett. 9, 315 (1969)].

[8] D. Gregg and S. Thomas, J. of Applied Optics 37, 2787 (1966).

[9] N. G. Basov, V. A. Gribkov, O. N. Krokhin, and G. V. Sklizkov, Zh. Eksp. Teor. Fiz. 54, 1073 (1968) [Sov. Phys. JETP 27, 575 (1968)].

[10] N. G. Basov, V. A. Boĭko, V. A. Gribkov, Yu. A. Drozhbin, S. M. Zakharov, O. N. Krokhin, G. V. Sklizkov, and V. A. Yakovlev, Metodika Skorostnykh Interferometricheskikh Izmereniĭ Raspredeleniya Plotnosti v Lazernoĭ Plazme (Methodology of High-speed Interferometric Measurements of Density Distribution in Laser Plasma). Preprint FIAN No. 79, 1970.

[11] V. A. Gribkov, V. Ya. Nikulin, and G. V. Sklizkov, Preprint FIAN No. 153, 1970.

[12] E. V. Aglitskiĭ, V. A. Boĭko, S. M. Zakharov, and G. V. Sklizkov, Preprint FIAN No. 143, 1970.

[13] N. G. Basov, V. A. Boĭko, Yu. A. Drozhbin, S. M. Zakharov, O. N. Krokhin, G. V. Sklizkov, and V. A. Yakovlev, Dokl. Akad. Nauk SSSR 192, 1248 (1970).